Nano Research 2017, 10(3): 1078–1091
DOI 10.1007/s12274-016-1368-3
Research Article
ISSN 1998-0124
CN 11-5974/O4

Ultra-fast microwave aided synthesis of gold nanocages and structural maneuver studies

Sreejith Raveendran[1], Anindito Sen[2], Toru Maekawa[1], and D. Sakthi Kumar[1] (✉)

[1] *Bio-Nano Electronics Research Centre, Graduate School of Interdisciplinary New Science, Toyo University, 2100, Kujirai, Kawagoe, Saitama 350-8585, Japan*
[2] *JEOL Ltd., 13F, Ohtemachi Nomura Building, 2-1-1 Ohtemachi Chiyoda-Ku., Tokyo 100-0004, Japan*

Received: 13 October 2016
Revised: 10 November 2016
Accepted: 11 November 2016

KEYWORDS
gold nanocages,
nanocages,
nanoboxes,
microwave technology,
ultra-fast,
screw dislocation

ABSTRACT

Gold nanocages (AuNcgs) are well-studied, hollow, metallic nanostructures that have fascinated researchers in the fields of nanotechnology, materials science, photoelectronics, biotechnology, and medical science for the last decade. However, the time-consuming synthesis of AuNcgs has limited their widespread use in materials science and nano-biotechnology. A novel, ultra-fast, simple, and highly convenient method for the production of AuNcgs using microwave heating is demonstrated herein. This quick method of AuNcg synthesis requires mild laboratory conditions for large-scale production of AuNcgs. The microwave heating technique offers the advantage of precise mechanical control over the temperature and heating power, even for the shortest reaction period (i.e., seconds). Microwave-synthesized AuNcgs were compared with conventionally synthesized AuNcgs. Structural maneuver studies employing the conventionally produced AuNcgs revealed the formation of screw dislocations and a shift in the lattice plane. Detailed characterization of the microwave-generated AuNcgs was performed using high resolution transmission electron microscopy (HRTEM), scanning electron microscopy (SEM), X-ray powder diffraction (XRD), and spectroscopic techniques.

1 Introduction

Gold (Au) nanostructures are indisputably versatile materials with applications in nanoscience, nanotechnology, biomedicine, and materials science [1–3]. Owing to their bio-inertness and multifaceted nature, these nanostructures have been studied relentlessly based on their methods of synthesis, structure, shape, crystallinity, size-tunability, surface functionalization, localized surface plasmon resonance (LSPR), biocompatibility, and other characteristics [4–8]. Among the synthesized Au nanostructures, Au nanocages (AuNcgs) are well-studied, hollow, nanoparticles with multifarious applications. AuNcgs were first synthesized and

Address correspondence to sakthi@toyo.jp

isolated by Sun and Xia, and have since become established as a multifunctional material for nanomedicine and material science applications [1, 6, 9, 10]. An effective polyol method for the synthesis of silver nanocubes (AgNcbs) was developed, where the AgNcbs were then employed as sacrificial templates for the galvanization reaction with $HAuCl_4$ solution to obtain AuNcgs [6, 11, 12]. The method required the use of syringe pumps, continuous magnetic stirring, and conventional heating equipment throughout the experiment. This conventional mode of synthesis utilizes simultaneous introduction of poly(vinylpyrrolidone) (PVP) and $AgNO_3$ solution into the reaction mixture via a two-channel syringe pump under constant magnetic stirring and heating, which is crucial to the success of the experiment. However, several modified methods were introduced in later years. Nevertheless, all of the conventional methods involve precise monitoring of several parameters, such as the proton concentration [13], temperature variation [14], reaction time [13], and shielding atmosphere [15, 16]. In order to overcome these relative difficulties, Chen et al. demonstrated a rapid protocol for microwave-assisted polyol synthesis of AgNcbs and Ag nanowires [17], and later several other researchers adopted this method as a more convenient and ultra-fast route for obtaining mono-disperse silver nanostructures [18].

Microwave-assisted synthesis of nanomaterials is of broad scientific interest owing to the fast and facile nature of this method, the controlled heating, reduced reaction time, and amenability to steady scale-up. Herein, we demonstrate a novel approach to the synthesis of Au-Ag alloy nanocages (hereafter denoted as AuNcgs-weight percentage of Au-94.42% and Ag-5.58%) from AgNcbs via a microwave-assisted rapid displacement method. The microwave-assisted quick synthesis of AgNcbs was performed as previously reported [17], and these species were then used as a sacrificial template in our exploration of the possibility of synthesizing AuNcgs using microwave heating. The method is highly convenient and rapid with the marked advantage of a decrease of the reaction time from several hours to a few seconds. The as-synthesized AuNcgs were characterized using high resolution transmission electron microscopy (HRTEM), energy dispersive spectroscopy (EDS), scanning electron microscopy (SEM), UV–visible (UV–Vis) spectroscopy, X-ray powder diffraction (XRD), X-ray photoelectron spectroscopy (XPS), and dynamic light scattering (DLS) for comparative analysis with the conventionally synthesized AuNcgs. This microwave-assisted synthesis method facilitates scale-up and mass production of AuNcgs that possess tremendous potential as contrast agents in non-linear optics, bioimaging, photothermal studies, drug delivery, and biosensing. Further, the conventionally synthesized AuNcgs were subjected to structural maneuver and beam damage studies by ultrasonication at high temperature and prolonged electron beam bombardment, respectively. TEM-based image dislocation studies of nanoparticles are widely used for understanding the crystal defects and changes in the atomic structure of nanoparticles [19, 20]. Atomic dislocations in the nanoparticles and their interactions can strongly influence several characteristic properties of the nanoparticles. These studies are expected to find applications in nanotechnology and materials science to further the development of robust nanomaterials.

2 Experimental

Synthesis of AgNcbs was performed via two different methods, i.e., the method introduced by Xia and coworkers [6, 10, 12] (conventional method) and that presented by Chen et al. [17] (microwave synthesis method). The thus-produced AgNcbs were used as the initial template for the production of AuNcgs. The AuNcgs were rapidly synthesized via a novel microwave-assisted method and were compared with conventionally synthesized AuNcgs. All chemicals were purchased from Sigma-Aldrich, unless otherwise specified. All other chemicals and reagents used were of analytical grade.

2.1 Synthesis of silver nanocubes

2.1.1 *Microwave-assisted synthesis of AgNcbs*

The microwave-assisted polyol method was used to synthesize AgNcbs for rapid and convenient production. According to Chen et al., the microwave-mediated nanocube synthesis reduces the more than 1 h reaction time required for the conventional

method to several minutes [17]. The experiment was conducted in a microwave oven (LG Electric, Japan, YJ-50H8) operating at a frequency of 50 Hz, with a power consumption of 1,000 W, rated high frequency output of 500 W, and rated voltage of 100 V. Briefly, 10 mL of a 250 μM ethylene glycol (EG; Kanto Chemicals, Japan) solution of Na_2S was vigorously stirred after adding 0.075 M PVP. The mixture was injected dropwise into 10 mL of an EG solution of $AgNO_3$ (0.05 M) (Kanto chemicals, Japan) under constant magnetic stirring by using a syringe. Upon addition of $AgNO_3$, the solution turned wine-red due to the formation of Ag_2S. The wine-red solution was intermittently heated (stop & start method) in a microwave and swirled manually for thorough mixing between the heating steps. Vaporization of the EG solution was prevented by the intermittent heating. The reaction was stopped when a khaki-colored solution containing AgNcbs formed. The AgNcbs were washed thoroughly using an acetone/water mixture (1:1) and with water, centrifuged, and sonicated before dispersing them in deionized water for further use.

2.1.2 *Conventional synthesis of AgNcbs*

Based on the experiments conducted by Xia and coworkers, the AgNcbs were produced via the polyol method under controlled conditions. The primary reaction in the synthesis of the AgNcbs involved the reduction of 0.25 M silver nitrate at 160 °C in a flask containing 5 mL of anhydrous EG and 0.19 M PVP. $AgNO_3$ and PVP were simultaneously added to the hot EG solution using a two-way syringe pump at a uniform rate of approximately of 45 $mL \cdot h^{-1}$. The reaction mixture was heated for another 40 min under constant magnetic stirring. Formation of the AgNcbs strongly depends on the reaction conditions and the concentration of $AgNO_3$ and PVP. A series of color changes were observed upon formation of the AgNcbs and silver plating could also be observed on the rim of the reaction flask. The final product appeared off-white or khaki colored. The reaction products were washed thoroughly using acetone, an acetone-water (1:1) mixture, and water, respectively. After several washings, the AgNcbs were dispersed in deionized water for synthesis of the AuNcgs.

2.2 Synthesis of AuNcgs

2.2.1 *Microwave-assisted synthesis of AuNcgs*

The displacement reaction was carried out using different volumes of 0.1 mM $HAuCl_4$ solution in a microwave oven (LG Electric, YJ-50H8, Japan). Different volumes (1.0, 1.5, 2.0, 2.5, 3.0, 3.5,4.0, 4.5, and 5 mL) of the 0.1 mM $HAuCl_4$ solution were respectively added to a mixture of 550 μL of as-synthesized AgNcbs in 5 mL of 9 mM aqueous solution of PVP. The mixture was intermittently heated in the microwave oven until a stable color was maintained. The absorbance was measured after each reaction. The AuNcgs were first washed with a saturated solution of NaCl to remove the AgCl residues and subsequently washed several times with water and an ethanol/water (1:1) mixture and dispersed in deionized water for characterization.

2.2.2 *Conventional synthesis of AuNcgs*

AuNcgs were synthesized according to the conventional method described by Skrabalak and coworkers [11]. Briefly, the AgNcbs synthesized via the conventional method were used for the galvanization reaction with $HAuCl_4$ solution to yield AuNcgs. The optimum concentration was determined based on the required position of the SPR peak in the near-infrared (NIR) window. The end product was first washed with a saturated solution of NaCl to remove the AgCl residue and then washed several times with water and then with an ethanol and water (1:1) mixture. Finally, the AuNcgs were dispersed in deionized water and stored in the dark for further use.

2.3 Structural maneuver studies

The AuNcgs synthesized via the conventional method were subjected to structural maneuver studies using high-frequency ultrasonication (45 Hz) at 60 °C for 30 min. Similarly, the electron-beam dependent atomic dislocations and morphological changes were analyzed by using HRTEM and SEM beam exposure studies, respectively. The HRTEM experiments were performed with continuous beam exposure for 20 min and images were recorded at 5 min intervals. The changes in the crystalline lattice and morphology were analyzed using

electron micrographs recorded in series followed by computational image analysis.

2.4 Characterization of AgNcbs and AuNcgs

AgNcbs and AuNcgs, synthesized by the respective methods, were compared and characterized using SEM, HRTEM, XPS, XRD, and EDS. SEM images were acquired using a Hitachi SU6600 instrument equipped with an EDS-51-XMX0017 apparatus (Oxford Instruments). Electron micrographs of the particles were recorded using TEMs JEM-2100 and HRTEM JEM-ARM200F operating at an accelerating voltage of 200 keV. UV–Vis absorption spectra of the as-synthesized AgNcbs and AuNcgs were measured with a Beckman Coulter spectrophotometer (DU730). XPS spectra were recorded using a Kratos-Axis-His Shimadzu instrument (Japan). XRD spectra were recorded using a RIGAKU, Smart Lab9kW instrument. BSoft [21], UCSF Chimera [22], and FIJI (image J) [23] software were used for image analysis.

3 Results and discussion

Monodisperse AgNcbs were synthesized using microwave-assisted heating, as demonstrated by Chen et al. [17]; the AgNcbs were then used as a sacrificial template for rapid synthesis of the AuNcgs. In the typical microwave-assisted displacement reaction, AgNcbs were mixed with PVP and the mixture was preheated prior to dropwise addition of the $HAuCl_4$ solution. The mixture was intermittently heated in a microwave oven using a start/stop method in order to avoid quick evaporation. The reaction was continued until a stable color (pale violet, which is typical for AuNcgs) was obtained. The duration of the reaction required to obtain a stable color varied from several seconds to 4 min based on the volume of the reaction mixture. The detailed experimental procedure is described in the Experimental section. After several experiments, the initial volume of the as-synthesized AgNcbs was optimized to 550 μL for the typical galvanization reaction with Au solution. Different volumes of 0.1 mM $HAuCl_4$ solution (1.0, 1.5, 2.0, 2.5, 3.0, 4.0, 4.5, and 5.0 mL) were respectively mixed with the AgNcbs (550 μL) and subjected to the microwave reaction. The optimum volume of 0.1 mM $HAuCl_4$ for producing uniform particle sizes was 5 ml, as determined by tuning the SPR peak in the near-NIR region. This optimized volume of $HAuCl_4$ solution produced AuNcgs with a practicable and excellent SPR absorption range in the near-NIR window, making them viable for future application in several biomedical applications, including imaging, therapy, and drug delivery [11, 24]. A higher heating power increases the reaction temperature and consequently increases the rate of the galvanic replacement reaction to generate porous, hollow AuNcgs. As reported previously [11], the displacement reaction starts from the highest energy site of the AgNcbs and Ag will be rapidly replaced with Au atoms, resulting in the formation of AuNcgs with predominant holes in the faces. As the reaction continues, reconstruction of the corners is initiated to form etched edges and pores in the corners [11].

By varying the volume of $HAuCl_4$ solution added to AgNcbs, AuNcgs with different degrees of hollowness were formed. Under the optimum conditions, the AgNcbs synthesized via the microwave method absorbed light in the range of 400–450 nm [11]; upon galvanic replacement with $HAuCl_4$ solution, the absorption shifted towards the near-NIR region. Figures 1(a)–1(h) shows SEM images of the AuNcgs synthesized via the microwave heating method with various volumes of $HAuCl_4$ solution. The UV–Vis spectra of the AuNcgs and the corresponding colored product formed during the reaction are shown in Figs. 1(j) and 1(k), respectively. Figure 1(l) shows a schematic diagram of the generation of the hollow nanocages from the solid nanocubes via microwave synthesis. The SEM images were recorded and the corresponding elemental mapping patterns were obtained for each batch of AuNcgs synthesized by the addition of different volumes of $HAuCl_4$ solution (Fig. 2). The weight percentage of the Ag atoms readily decreased with respect to the Au atoms as the galvanic replacement reaction proceeded with increasingly higher volumes of $HAuCl_4$ solutions. The rate of Au deposition increased as the volume of the $HAuCl_4$ solution increased from 1.0 to 5.0 mL. Pores started to appear on the surface and corners of the AgNcbs as the displacement reaction proceeded. The reaction

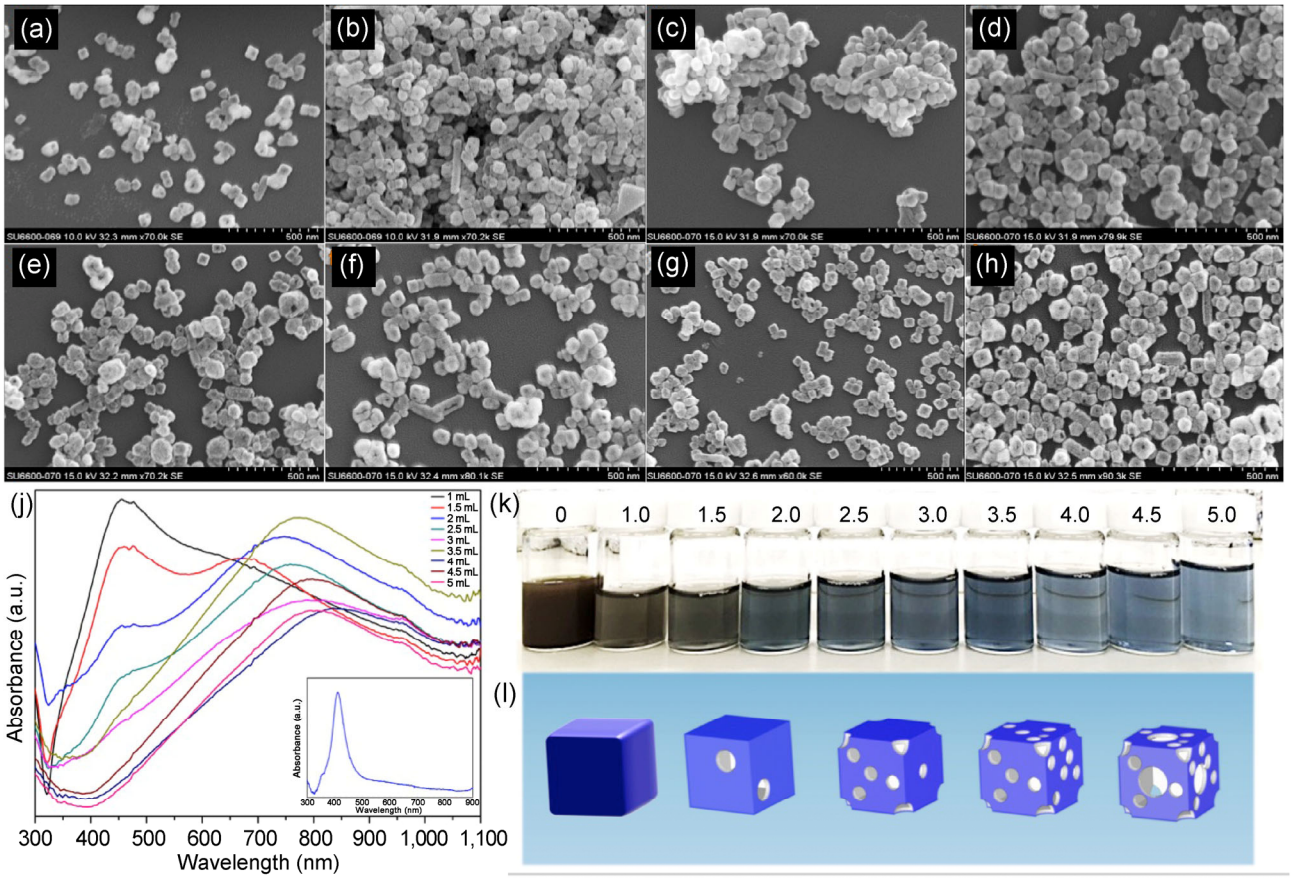

Figure 1 (a)–(h) SEM image of AgNcbs synthesized using microwave method by adding different volume of $HAuCl_4$ solution: (a) 1.0, (b) 1.5, (c) 2.0, (d) 2.5, (e) 3.0, (f) 3.5, (g) 4.0, and (h) 4.5 mL. (i) UV–Vis absorption spectra for AuNcgs synthesized via microwave synthesis by adding different volumes of $HAuCl_4$ solution; UV–Vis spectra for AgNcbs synthesized via microwave heating (inset of (j)). (k) Photograph showing the reaction products after each microwave experiment. (l) Computationally generated 3D schematic maps resembling the different stages of hollow nanocages formed from solid nanocubes via microwave synthesis.

with 5.0 mL of $HAuCl_4$ solution produced excellent, hollow, porous AuNcgs with an SPR peak in the range of 800–1,100 nm. The hollow AuNcgs exhibited interesting optical properties directly related to the SPR peak, which in turn depends on the morphology of the nanocages [9].

Figure 3 presents the HRTEM data and EDS images of the AgNcbs and AuNcgs produced via ultra-fast microwave synthesis. Figures 3(a) and 3(i) show the low magnification bright field TEM images of the AgNcbs and AuNcgs, respectively. Corresponding photographs of the respective solutions are presented in the insets of the figures. The data show the successful galvanic replacement of Ag atoms by Au to form the hollow nanocages. Figures 3(b) and 3(j) respectively show the high angle annular dark field-scanning transmission electron microscopy (HAADF-STEM) images of AgNcbs and AuNcgs respectively. Comparison the typical TEM image of AgNcb in Fig. 3(d) with that of AgNcb in Fig. 3(b) clearly demonstrates that a small amount of etching occurred during exposure of the sample to the electron beam while recording the high resolution HAADF-STEM image. Slight rounding of the corners of the AgNcbs can be clearly observed in Fig. 3(b), as compared with the edges of the nanocubes shown in Fig. 3(d). As suggested by Skrabalak et al., this rounding can be attributed to electron beam damage, which causes slight dissolution of the Ag atoms at the cube corners due to the strong interaction of the stabilizing agent, PVP, with the {100} facets of Ag [10]. Excessive bombardment of the sample with the electron beam

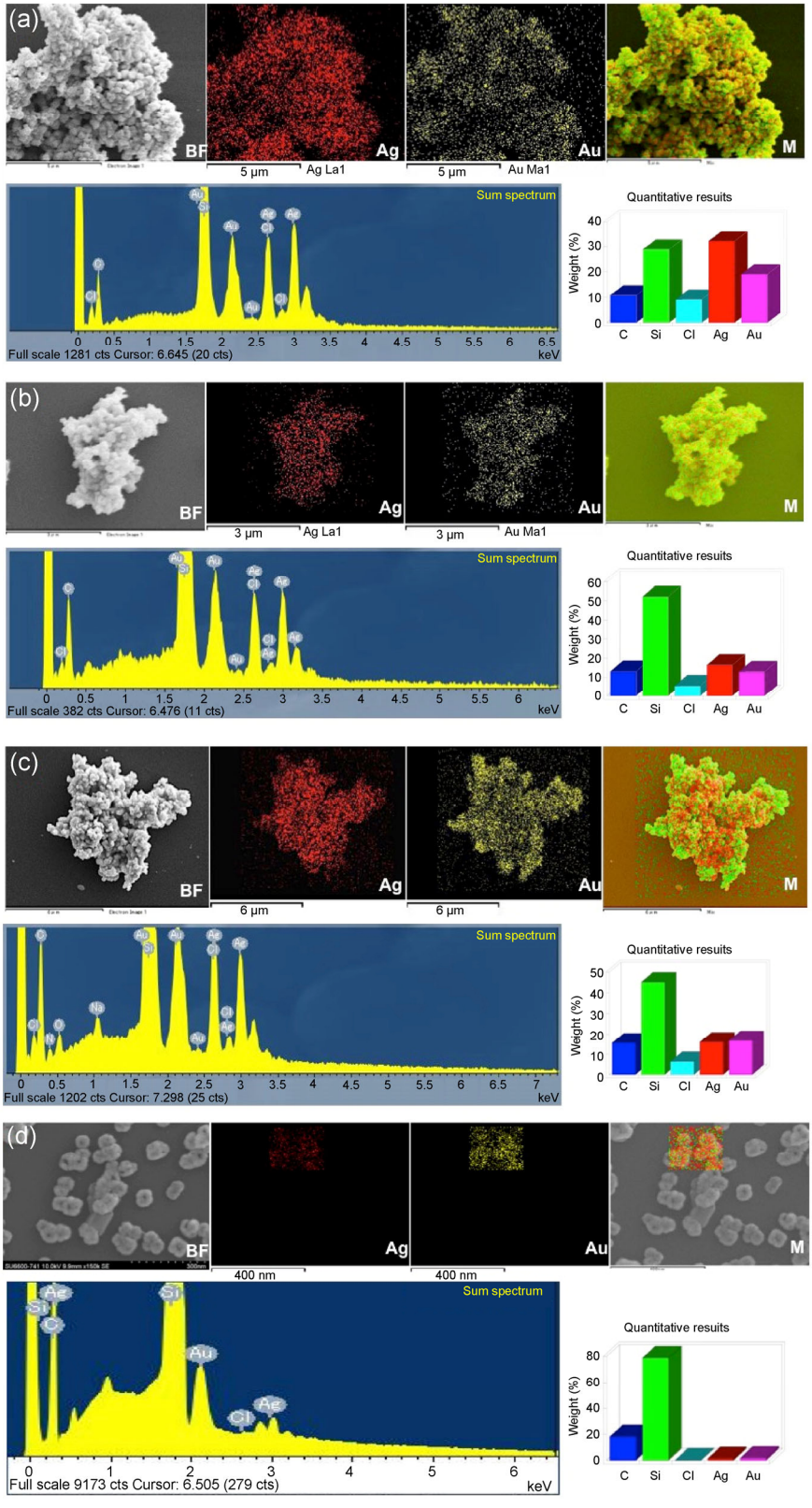

Figure 2 SEM image and EDS mapping of Ag/AuNcgs synthesized using microwave method, bright field (BF) image, Ag map, Au map and merged map followed by EDS spectra showing elemental composition and element weight percentage graph. SEM mapping images are recorded on the basis of the volume of 0.1 mM $HAuCl_4$ which was added to the galvanic replacement reaction: (a) 1.5, (b) 2.0, (c) 3.0 and (d) 5.0 mL.

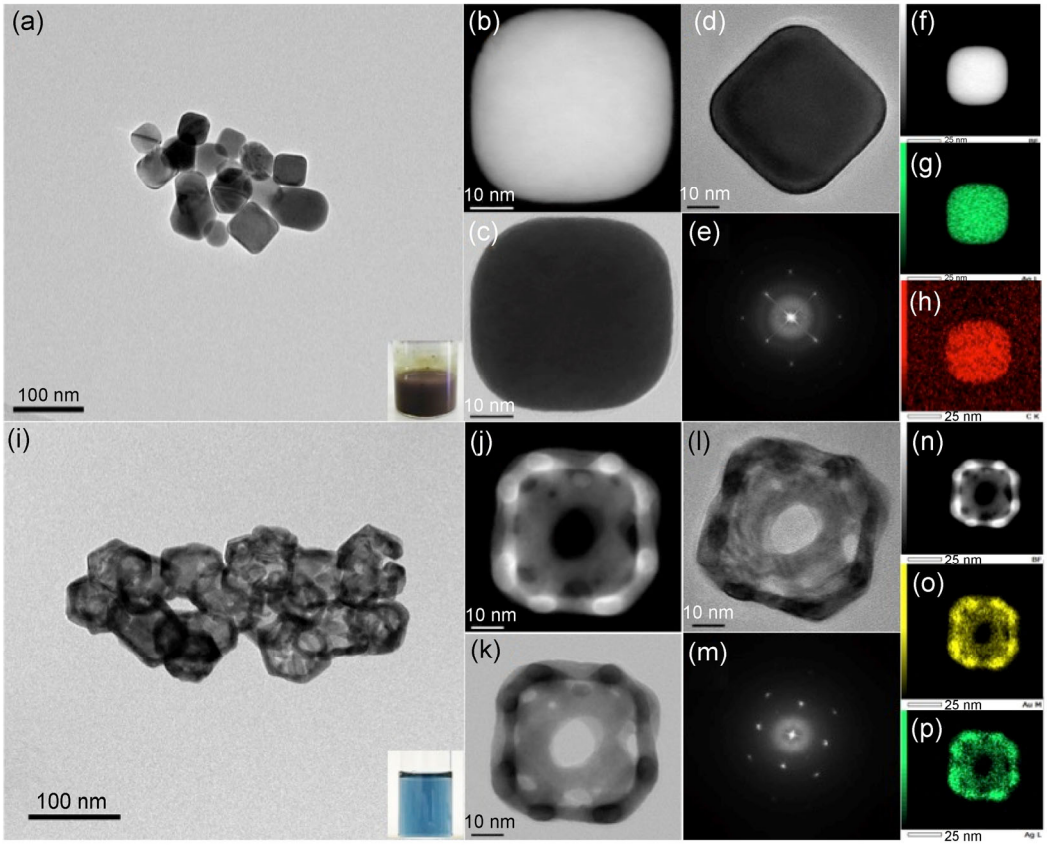

Figure 3 HRTEM characterization of AgNcbs and AuNcgs synthesized via microwave technology: (a) low magnification TEM image of cluster AgNcbs synthesized using microwave method, photograph of AgNcbs synthesized in the inset; (b) HAADF-STEM image of AgNcbs synthesized using microwave oven method; (c) corresponding high magnification bright field TEM image of AgNcb; (d) normal TEM image of AgNcb recorded before taking HAADF-STEM imaging; (e) corresponding FFT image of AgNcb; (f)–(h) EDS mapping images of AgNcb (BF, Ag and C mappings); (i) low magnification TEM image of cluster AuNcgs synthesized using microwave method, photograph of AuNcgs synthesized in the inset; (j) HAADF-STEM image of AuNcgs synthesized using microwave oven method; (k) corresponding high magnification BF TEM image of AuNcg; (l) normal TEM image of AuNcg recorded before taking HAADF-STEM imaging; (m) corresponding FFT image of AuNcg; (n)–(p) EDS mapping image of AuNcgs (BF, Au and Ag mappings).

during high-resolution imaging and HAADF-STEM recording causes slight modification of the cube corners due to the uneven coating of PVP on the AgNcb surfaces. As reported previously, AgNcbs with sharp corners have equally passivated surfaces of PVP that prevent easy dissolution of the weakly bound Ag atoms in the corners and prevents rounding of the AgNcbs [10]. Figure 3(e) shows the fast Fourier transform (FFT) pattern of the {100} plane of the face-centered cubic (fcc) AgNcbs. The EDS mapping images of AgNcbs in Figs. 3(f)−3(h) indicate the purity of the nanocubes with silver and carbon derived from PVP. Similarly, the purity of the AgNcbs was confirmed by the XRD analysis, as discussed later in this paper. Deposition of Au occurs along with the dissolution of the unprotected Ag atoms in the corners of the nanocubes, resulting in the formation of hollow AuNcgs with holes on the faces and corners. In the conventional synthesis, the addition of a small volume of $HAuCl_4$ solution (starting from 0.5 to 5 mL) initializes the displacement reaction by pin-hole formation on the high-energy site on the surface of the AgNcbs; the addition of 5 mL of $HAuCl_4$ solution induces complete dealloying, resulting in fragmentation of the AuNcgs [25]. Under microwave conditions, visible pinhole formation started on the surface of the AgNcbs with the addition of a lower volume of $HAuCl_4$ solution, and pinhole development increased rapidly with the

addition of higher volumes. As the volume of the $HAuCl_4$ solution increased, the displacement reaction increased, leading to the formation of more uniform holes on the faces and corners of the nanocubes. By fine-tuning the SPR peak to the most convenient window of the near-NIR region by adding 5 mL of 0.1 mM $HAuCl_4$ solution, we were able to harvest AuNcgs with a uniform size and with holes on the faces (edge length ≈ 70 nm). The high resolution HAADF-STEM image of the AuNcgs presented in Fig. 3(j) clearly demonstrates that the pores are localized on every face of the hollow nanocages and in the corners as well. The dealloying process is initiated at the surfaces of the AgNcbs and extends to the corners. Because the reaction under microwave conditions occurs at an ultrafast rate, the dealloying process was completed within a few seconds. The electron micrograph images show that the holes generated as a result of galvanic replacement of Ag were simply amorphic compared to the square patterned holes formed in the nanocages developed via the conventional method [25]. The nanocages synthesized using the conventional method show holes with a square pattern on the surfaces (Fig. S1 in the Electronic Supplementary Material (ESM)). The transformation of the pinholes to square patterned holes on the surface of the nanocages during the displacement reaction was attributed to the square arrangement of the atoms on each wall where the surface has a {100} crystallographic plane [25].

Figure 4 presents the SEM, XRD, DLS, and XPS characterization of the AgNcbs and AuNcgs optimized by adding 5 mL of 0.1 mM $HAuCl_4$ solution in the microwave-assisted synthesis. Figures 4(a) and 4(b) show the SEM images of the pure AgNcbs isolated after several washings. Figure 4(c) shows the corresponding XRD pattern of the AgNcbs used for production of the AuNcgs. The five most prominent diffractions peaks were indexed to the (111), (200), (220), (311), and (222) planes of pure fcc silver crystals [6, 17]. The XRD spectrum of the AgNcbs demonstrates that the nanocubes harvested and used for nanocage synthesis were pure and devoid of any impurities as no other diffraction peaks were observed during the analysis. The intensity of the (111) peak was relatively high compared to that of the (200) peak, indicating a slightly truncated cube morphology [26]. Similarly, the intensity ratio of the (200) and (111) peaks of the AgNcbs was comparable with the conventional value (0.35 versus 0.4), which indicates the abundance of nanocubes with {100} facets. The slight decrease in the experimental ratio can be attributed to the texturing effects of these nanocubes on the flat substrate [27, 28]. The strong (220) peak is ascribed to the substantial number of {110} facets on the nanocubes [26]. Figures 4(d) and 4(e) show the SEM images of the hollow AuNcgs with uniformly distributed pores on the faces and corners. Similarly, the XRD spectra of the AuNcgs show a strong (111) peak compared to the (200) and (220) peaks (Fig. 4(f)). However, the ratio of the peak intensities for the (200) to (111) peaks is smaller than that for Au in the conventional bulk sample (0.34 versus 0.52), showing that the ratio decreases with an increase in the particle size [29]. A slight increase in the size of the AuNcgs was observed after the galvanic replacement reaction. Peaks from AgCl crystals along with those from the AuNcgs were present in the XRD plots recorded for the AuNcgs. This is due to the presence of AgCl residue produced during the displacement reaction even after thorough washing with saturated NaCl solution [11, 25]. Figure 4(g) shows the DLS data for the AuNcgs. Figures 4(h) and 4(i) show the XPS spectra for Ag and Au in the AgNcb and AuNcg samples, respectively. Figure 4(h) shows the Ag $3d_{5/2}$ peak at 368.4 eV and Fig. 4(i) shows the Au $4F_{7/2}$ peak at 83.7 eV.

Structural maneuver studies were performed to evaluate the robustness (rigidity and inertness) of the nanocages along with that of the conventionally synthesized AuNcgs for biomedical applications including multimodal imaging and photothermal therapy. TEM images of the conventionally synthesized AuNcgs with their respective EDS mapping patterns and spectra are presented in Fig. S2 (in the ESM), along with that of the microwave-synthesized AuNcgs. The particles were polydisperse with sizes ranging from 35 to 500 nm. The HRTEM images were recorded for smaller AuNcgs produced via the conventional synthesis to analyze the crystalline lattice pattern (Fig. S3 in the ESM). In the conventional method of synthesis, addition of 1.5 mL of $HAuCl_4$ solution

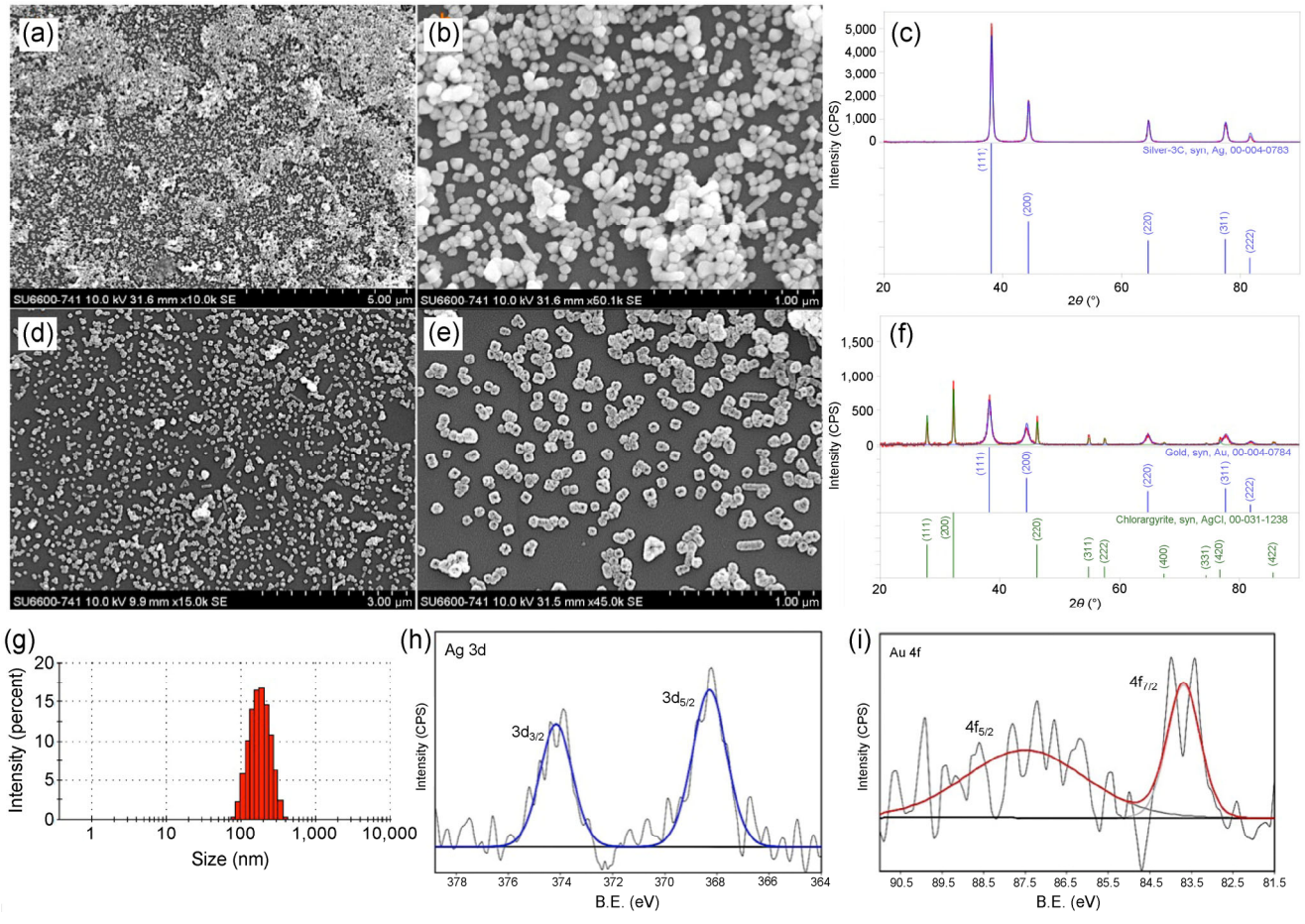

Figure 4 (a) and (b) SEM images of AgNcbs synthesized using microwave method. (c) XRD spectra of AgNcbs synthesized using microwave oven method showing the peaks (111), (200), (220), (311) and (222) compared with JCPDS file for Ag (00-004-0783). (d) and (e) SEM images of AuNcgs synthesized using microwave method, showing holes in the centre of AuNcg faces. (f) XRD spectra of AuNcgs synthesized using microwave oven method showing the peaks (111), (200), (220), (311) and (222) compared with JCPDS file for chlorargyrite, AgCl (00-031-1238). (g) DLS measurement graph showing the size distribution of AuNcgs synthesized via microwave method. (h) XPS spectra of silver measured from AgNcbs. (i) XPS spectra of Au measured from AuNcgs.

produced nanocages with holes on the corners and surfaces. However, the holes were not uniformly found on all four facets of the nanocages (Figs. S1(c) and S1(d) in the ESM). Atomic level characterization using HRTEM was performed for the AuNcgs and Ag/Au twinned nanoparticles produced during the incomplete galvanization reaction via the conventional method with a lower volume of $HAuCl_4$ solution. Identification of the lattice planes of the twinned nanoparticles via HRTEM characterization revealed that the conventionally produced nanocages have twin boundaries. The *d*-spacing of 2.36 Å corresponds to the (111) plane of fcc gold, showing the presence of twinned particles abundant with (111) crystalline planes, in addition to cubic nanocages [29]. These nanoparticles were used for the structural maneuver studies using two different approaches; the primary approach employed HRTEM imaging and the second method employed SEM imaging.

In the HRTEM (JEM-ARM200F) analysis, the AuNcgs were exposed to the electron beam for a duration of 20 min at an accelerating voltage of 200 keV at a rate of 5.1 Columbs·cm^{-2} (dose density per 2 s exposure). Images were recorded periodically at an interval of 5 min. Care was taken to check for any movement of the particles during their exposure to the electron beam, which, gratifyingly, was negligible and nearly undetectable, owing to the stability of the TEM

system. The recorded images were then subjected to computational image analysis with software including BSOFT [21] and FIJI [23]. The series of five images recorded within a span of 20 min revealed that parts of the edge of the AuNcgs had suffered screw dislocation as a result of beam damage. The defect was clearly evident when the micrographs recorded at the 0th and 20th min of the exposure were compared (Figs. 5(a) and 5(d)). The red arrow and the blue line indicate the uniform inclined arrangement of the Au atoms in the undamaged state (Fig. 5(b)). A linear plot of the density variation (grey value), generated using software package FIJI [23], along the red line is shown in Fig. 5(c); the minimum is shown, indicating that the space between two adjacent Au atoms (marked by white arrows) lies around a grey value of 50 arbitrary units (a.u.). When the same analysis was carried out on the damaged region of the particle (Figs. 5(d) and 5(e)), the gap between the atoms decreased and the minimum of the linear density (the grey value) profile (Fig. 5(f)) along the red line (Fig. 5(e)) was much above 50 a.u., strongly suggesting rearrangement of the Au atoms due to beam damage. The maximum damage was suffered by a small set of Au atoms, as shown by the small green arrow, resulting in a zigzag pattern of atomic dislocations, a characteristic feature of screw dislocation [30]; the yellow and brown arrow with the small white arrowhead shows the maximum displacement (Fig. 5(e)). This displacement is measured using the program "bshow" included in the BSOFT software package. The view along the yellow arrow (Fig. 5(e)) reveals a slight shift (white arrow head) at the stacking-fault in the (111) plane. The lattice spacing in Au with the closest atomic approach is reported as 2.874 Å [31]. Herein, from the atomic resolution TEM image

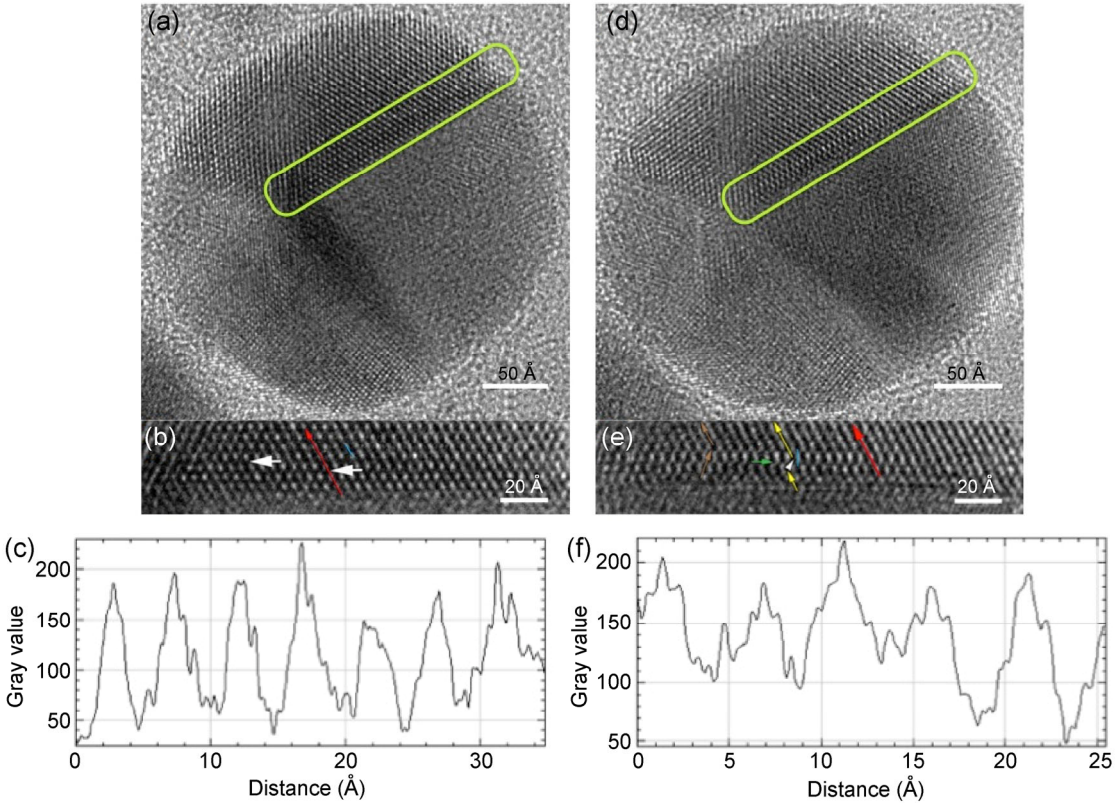

Figure 5 Electron beam damage study and HRTEM characterization of traditionally synthesized AuNcgs. (a) HRTEM image of AuNcg before prolonged beam bombardment (0th min), scale bar: 50 Å. (b) Lattice fringes—HRTEM image of AuNcg before prolonged beam bombardment (0th min) showing correct crystal lattice pattern, scale bar: 20 Å. (c) Linear density profile of (b) along the red line. (d) HRTEM image of AuNcg after prolonged beam bombardment (20th min) showing screw dislocation, zigzag lattice pattern, scale bar: 20 Å. Sighting along the yellow arrow reveals the slight shift at the stacking fault (white arrow head). (f) Linear density profile of (e) along the red line.

(Fig. 5(e)), it was observed as 2.8 Å, which corresponds to the {110} plane [32]. The width of the screw dislocation was found to be 1.8 Å. The stacking fault defect is associated with an increase in energy that produces a dissociation width of approximately 1 nm for screw dislocations in Au [20]. Due to the high surface energy and inhomogeneity in cube passivation, atoms located at the corners and edges become dislocated, which will increase the number of {111} facets, leading to the formation of truncated cubes or cages with the benefit of minimized surface energy [33]. This effect can be possibly attributed to the heating effect of the AuNcgs upon prolonged exposure to the electron beam, leading to an increase in the surface energy. According to Li et al., LSPR hybridization of cubic systems concentrates the surface charge on the cube corners, edges, and faces [34]. These unique properties of plasmonic nanoparticles have been well exploited in photothermal cancer therapy [35].

In another experiment, the conventionally synthesized AuNcgs were subjected to high-power ultrasonication for 30 min at a temperature of 60 ˚C, followed by morphological characterization using SEM imaging. The AuNcgs showed certain structural distortions and crystalline damages upon ultrasonication and upon continuous electron beam bombardment. The edges of the nanocages formed during galvanic replacement of Ag by Au exhibited a slight truncation [12], which increased during sonication at 60 ˚C for 30 min to show a clear demarcation with protruding faces (Fig. 6). Several interesting morphologies of the AuNcgs were observed during this experiment (Figs. S4 and S5 in the ESM). Release of the loosely bound polymer to reach the surface of the nanocages through the holes on the surface was observed from the SEM images (Fig. S4(f) in the ESM). Figures 7(a)–7(d) shows the series of images recorded at an interval of 1 min after continuous exposure to the electron beam in the SEM instrument for 5 min. The polymer present inside the nanocage was gradually released through the hole on the surface from the first minute to the fourth minute of electron beam exposure, with subsequent saturation. This indicates heating of the nanocage by electron beam irradiation, which in turn affects the weaker passivated area of the nanocage to release the enclosed polymer from the hollow interior. This property can be explored for drug delivery applications in several targeted therapies for site-directed drug release [9, 36,37]. Similarly, Figs. 7(e)–7(h) shows the change in the edge morphology of the nanocages upon continuous exposure of the nanocage to the electron beam. The data in Figs. 7(e)–7(h) confirm that the truncated edges and corners are more prone to electron beam damage than the nanocage facets, as the loosely bound polymers are more prone to dissolution and corrugation [10].

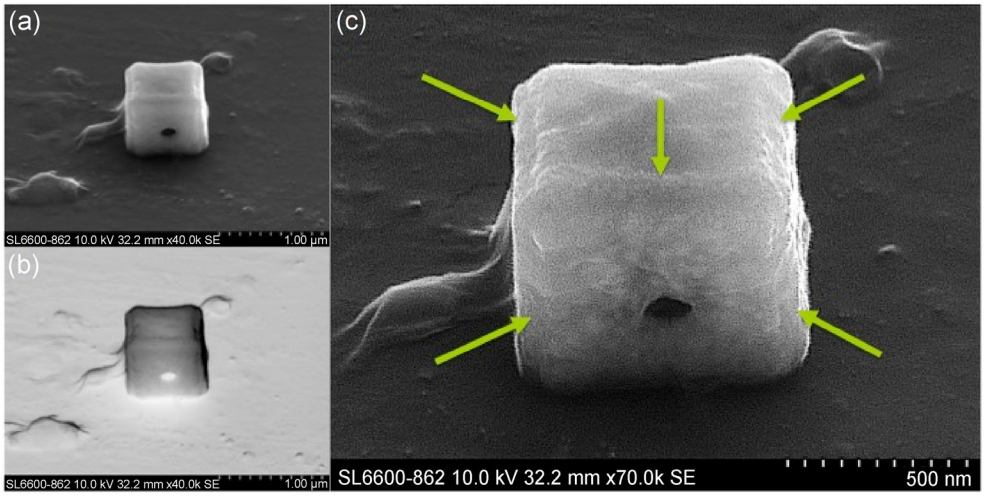

Figure 6 SEM characterization of traditionally synthesized and ultra sonicated AuNcg: (a) SEM image of AuNcg showing clear hole on the face of AuNcg tilted at an angle of 60°; (b) inverted α-SEM image of AuNcg showing clear hole on the face of AuNcg and well defined morphology; (c) magnified SEM image of AuNcg showing the corner truncation (arrows) on the edges of AuNcg.

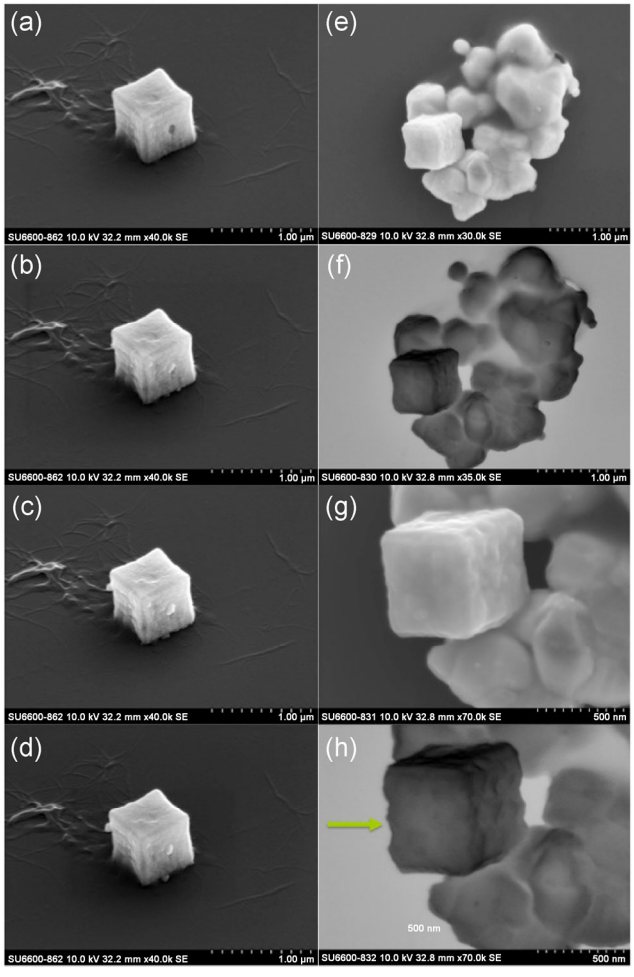

Figure 7 SEM characterization of AuNcgs synthesized via traditional method and structure maneuver. (a)–(d) Series of SEM images of AuNcgs recorded after electron beam exposure continuously and image recorded at an interval of 1 min each. Images (a)–(d) show the slow-release of loosely bound PVP through the hole on the surface of AuNcg on contrinuous beam exposure. (e) Low magnification SEM image of AuNcgs. (f) α-Inverted SEM image of AuNcgs. (g) Magnified image before beam exposure study. (h) α-Inverted image after 5 min beam exposure study. Arrow indicates the beam damage caused to the edge of the nanocage during prolonged electron beam exposure.

4 Conclusions

In summary, a high-speed microwave heating method was introduced for large-scale, facile and rapid production of monodisperse AuNcgs. This one-pot reaction produces AuNcgs with a cubic morphology at an ultra-fast rate compared to conventionally established synthesis methods. The method offers several advantages, including simplicity, a rapid reaction rate, mild laboratory conditions, large-scale productivity, and precise mechanical monitoring of the temperature and power. Similarly, it was demonstrated that the nanocages could be structurally manipulated by ultrasonication at a higher temperature for 30 min. The electron beam exposure study indicated possible beam/radiation damage, leading to structural variation of the AuNcgs with less homogeneous passivation with PVP. Thus, considering the versatility and ease, microwave-heating technology can be extensively applied for the scalable industrial production of AgNcbs and AuNcgs as an alternative to conventional heating methods. Owing to the potential applications of metal nanocages in nanomedicine and biomedical technology, AuNcgs produced via microwave technology should be subjected to more in-depth studies in the near future.

Acknowledgements

Authors would like to acknowledge their sincere gratitude to the Ministry of Education, Culture, Sports, Science and Technology (MEXT), Japan for the financial support under the program of the strategic research foundation at private universities S1101017, organized by the MEXT, Japan. S. R. would like to acknowledge Mr. Keiichi Yanagisawa for his sincere help extended for electron beam damage study and capturing HRTEM images using JEM-ARM200F.

Electronic Supplementary Material: Supplementary material (SEM, HRTEM, and EDS characterization for microwave synthesized AuNcgs and traditionally synthesized AuNcgs) is available in the online version of this article at http://dx.doi.org/10.1007/s12274-016-1368-3.

References

[1] Xia, X. H.; Xia, Y. N. Gold nanocages as multifunctional materials for nanomedicine. *Front. Phys.* **2014**, *9*, 378–384.

[2] Cobley, C. M.; Chen, J. Y.; Cho, E. C.; Wang, L. V; Xia, Y. N. Gold nanostructures: A class of multifunctional materials for biomedical applications. *Chem. Soc. Rev.* **2011**, *40*, 44–56.

[3] Jain, S.; Hirst, D. G.; O'Sullivan, J. M. Gold nanoparticles as novel agents for cancer therapy. *Br. J. Radiol.* **2012**, *85*, 101–113.

[4] Sajanlal, P. R.; Sreeprasad, T. S.; Samal, A. K.; Pradeep, T. Anisotropic nanomaterials: Structure, growth, assembly, and functions. *Nano Rev.* **2011**, *2*, 5883.

[5] Sun, Y.; Mayers, B.; Xia, Y. Metal nanostructures with hollow interiors. *Adv. Mater.* **2003**, *15*, 641–646.

[6] Sun, Y. G.; Xia, Y. N. Shape-controlled synthesis of gold and silver nanoparticles. *Science* **2002**, *298*, 2176–2179.

[7] Raveendran, S.; Chauhan, N.; Palaninathan, V.; Nagaoka, Y.; Yoshida, Y.; Maekawa, T.; Kumar, D. S. Extremophilic polysaccharide for biosynthesis and passivation of gold nanoparticles and photothermal ablation of cancer cells. *Part. Part. Syst. Charact.* **2015**, *32*, 54–64.

[8] Vigderman, L.; Khanal, B. P.; Zubarev, E. R. Functional gold nanorods: Synthesis, self-assembly, and sensing applications. *Adv. Mater.* **2012**, *24*, 4811–4841.

[9] Chen, J.; Wiley, B.; Li, Z. Y.; Campbell, D.; Saeki, F.; Cang, H.; Au, L.; Lee, J.; Li, X.; Xia, Y. Gold nanocages: Engineering their structure for biomedical applications. *Adv. Mater.* **2005**, *17*, 2255–2261.

[10] Skrabalak, S. E.; Chen, J. Y.; Sun, Y. G.; Lu, X. M.; Au, L.; Cobley, C. M.; Xia, Y. N. Gold nanocages: Synthesis, properties, and applications. *Acc. Chem. Res.* **2008**, *41*, 1587–1595.

[11] Skrabalak, S. E.; Au, L.; Li, X. D.; Xia, Y. N. Facile synthesis of Ag nanocubes and Au nanocages. *Nat. Protoc.* **2007**, *2*, 2182–2190.

[12] Chen, J. Y.; McLellan, J. M.; Siekkinen, A.; Xiong, Y. J.; Li, Z. Y.; Xia, Y. N. Facile synthesis of gold-silver nanocages with controllable pores on the surface. **2006**, *128*, 14776–14777.

[13] Im, S. H.; Lee, Y. T.; Wiley, B.; Xia, Y. N. Large-scale synthesis of silver nanocubes: The role of HCl in promoting cube perfection and monodispersity. *Angew. Chem., Int. Ed.* **2005**, *44*, 2154–2157.

[14] Sun, Y. G.; Yin, Y. D.; Mayers, B. T.; Herricks, T.; Xia, Y. N. Uniform silver nanowires synthesis by reducing $AgNO_3$ with ethylene glycol in the presence of seeds and poly(vinyl pyrrolidone). *Chem. Mater.* **2002**, *14*, 4736–4745.

[15] Chen, C.; Wang, L.; Jiang, G. H.; Zhou, J. F.; Chen, X.; Yu, H. J.; Yang, Q. Study on the synthesis of silver nanowires with adjustable diameters through the polyol process. *Nanotechnology* **2006**, *17*, 3933–3938.

[16] Lee, Y. T.; Im, S. H.; Wiley, B.; Xia, Y. N. Quick formation of single-crystal nanocubes of silver through dual functions of hydrogen gas in polyol synthesis. *Chem. Phys. Lett.* **2005**, *411*, 479–483.

[17] Chen, D. P.; Qiao, X. L.; Qiu, X. L.; Chen, J. G.; Jiang, R. Z. Convenient, rapid synthesis of silver nanocubes and nanowires via a microwave-assisted polyol method. *Nanotechnology* **2010**, *21*, 025607.

[18] Zhao, T.; Fan, J. B.; Cui, J.; Liu, J. H.; Xu, X. B.; Zhu, M. Q. Microwave-controlled ultrafast synthesis of uniform silver nanocubes and nanowires. *Chem. Phys. Lett.* **2011**, *501*, 414–418.

[19] Chen, C.-C.; Zhu, C.; White, E. R.; Chiu, C.-Y.; Scott, M. C.; Regan, B. C.; Marks, L. D.; Huang, Y.; Miao, J. W. Three-dimensional imaging of dislocations in a nanoparticle at atomic resolution. *Nature* **2013**, *496*, 74–77.

[20] Balk, T. J.; Hemker, K. J. High resolution transmission electron microscopy of dislocation core dissociations in gold and iridium. *Philos. Mag. A* **2001**, *81*, 1507–1531.

[21] Heymann, J. B.; Belnap, D. M. Bsoft: Image processing and molecular modeling for electron microscopy. *J. Struct. Biol.* **2007**, *157*, 3–18.

[22] Pettersen, E. F.; Goddard, T. D.; Huang, C. C.; Couch, G. S.; Greenblatt, D. M.; Meng, E. C.; Ferrin, T. E. UCSF chimera—A visualization system for exploratory research and analysis. *J. Comput. Chem.* **2004**, *25*, 1605–1612.

[23] Schindelin, J.; Arganda-Carreras, I.; Frise, E.; Kaynig, V.; Longair, M.; Pietzsch, T.; Preibisch, S.; Rueden, C.; Saalfeld, S.; Schmid, B. et al. Fiji: An open-source platform for biological-image analysis. *Nat. Methods* **2012**, *9*, 676–682.

[24] West, J. L.; Halas, N. J. Engineered nanomaterials for biophotonics applications: Improving sensing, imaging, and therapeutics. *Annu. Rev. Biomed. Eng.* **2003**, *5*, 285–292.

[25] Sun, Y.; Xia, Y. Mechanistic study on the replacement reaction between silver nanostructures and chloroauric acid in aqueous medium. *J. Am. Chem. Soc.* **2004**, *126*, 3892–3901.

[26] Lyu, L. M.; Wang, W. C.; Huang, M. H. Synthesis of Ag_2O nanocrystals with systematic shape evolution from cubic to hexapod structures and their surface properties. *Chem.—Eur. J.* **2010**, *16*, 14167–14174.

[27] Siekkinen, A. R.; Mclellan, J. M.; Chen, J.; Xia, Y. Rapid synthesis of small silver nanocubes by mediating polyol reduction with a trace amount of sodium sulfide or sodium hydrosulfide. *Chem. Phys. Lett.* **2006**, *432*, 491–496.

[28] Lee, C. F.; Chang, C. L.; Yang, J. C.; Lai, H. Y.; Chen, C. H. Morphological determination of face-centered-cubic metallic nanoparticles by X-ray diffraction. *J. Colloid Interface Sci.* **2012**, *369*, 129–133.

[29] Kwon, K.; Lee, K. Y.; Lee, Y. W.; Kim, M.; Heo, J.; Ahn, S. J.; Han, S. W. Controlled synthesis of icosahedral gold nanoparticles and their surface-enhanced Raman scattering property. *J. Phys. Chem. C* **2007**, *111*, 1161–1165.

[30] Chen, C.-C.; Zhu, C.; White, E. R.; Chiu, C.-Y.; Scott, M. C.; Regan, B. C.; Marks, L. D.; Huang, Y.; Miao, J. W. Three-dimensional imaging of dislocations in a nanoparticle at atomic resolution. *Nature* **2013**, *496*, 74–77.

[31] Davey, W. P. Precision measurements of the lattice constants of twelve common metals. *Phys. Rev.* **1925**, *25*, 753–761.

[32] Liu, S. J.; Zheng, X. S.; Song, L.; Liu, W.; Yao, T.; Sun, Z. H.; Lin, Y.; Wei, S. Q. Partial-surface-passivation strategy for transition-metal-based copper-gold nanocage. *Chem. Commun.* **2016**, *52*, 6617–6620.

[33] Huang, R.; Wen, Y.-H.; Shao, G.-F.; Zhu, Z.-Z.; Sun, S.-G. Single-crystalline and multiple-twinned gold nanoparticles: An atomistic perspective on structural and thermal stabilities. *RSC Adv.* **2014**, *4*, 7528–7537.

[34] Li, G.; Cherqui, C.; Bigelow, N. W.; Duscher, G.; Straney, P. J.; Millstone, J. E.; Masiello, D. J.; Camden, J. P. Spatially mapping energy transfer from single plasmonic particles to semiconductor substrates via STEM/EELS. *Nano Lett.* **2015**, *15*, 3465–3471.

[35] Morton, J. G.; Day, E. S.; Halas, N. J.; West, J. L. Nanoshells for photothermal cancer therapy. In *Cancer Nanotechnology*; Grobmyer, S. R.; Moudgil, B. M., Eds.; Humana Press: New York, 2010; pp 101–117.

[36] Yavuz, M. S.; Cheng, Y. Y.; Chen, J. Y.; Cobley, C. M.; Zhang, Q.; Rycenga, M.; Xie, J. W.; Kim, C.; Song, K. H.; Schwartz, A. G. et al. Gold nanocages covered by smart polymers for controlled release with near-infrared light. *Nat. Mater.* **2009**, *8*, 935–939.

[37] Li, W. Y.; Cai, X.; Kim, C.; Sun, G. R.; Zhang, Y.; Deng, R.; Yang, M. X.; Chen, J. Y.; Achilefu, S.; Wang, L. V. et al. Gold nanocages covered with thermally-responsive polymers for controlled release by high-intensity focused ultrasound. *Nanoscale* **2011**, *3*, 1724–1730.